Substituent Effects on the Adsorption of Dialkyl Sulfides on Gold Nanoparticles

David B. Pedersen* and Scott Duncan*

Defence R&D Canada-Suffield, P.O. Box 4000 Station Main, Medicine Hat, Alberta, Canada T1A 8K8

Received: July 12, 2005; In Final Form: September 2, 2005

The adsorption of chloroethyl ethyl sulfide and 2,2′-dichloro ethyl sulfide to gold nanoparticles has been examined in the gas phase using surface-plasmon resonance spectroscopy. The equilibrium constants for the gas-phase adsorption reactions are 14 ± 4 and 25 ± 5 atm^{-1}, respectively. The bond energy of the Au−chloroethyl ethyl sulfide complex is 44 ± 9 kJ mol^{-1}. The bond energy of Au−2,2′-dichloro ethyl sulfide is estimated to be 47 kJ mol^{-1}. Halogenation of the dialkyl side chains is found to have little impact on the chemistry, and only physisorption processes occur, analogous to dialkyl sulfide adsorption on Au surfaces.

1. Introduction

The affinity of sulfur for noble metals has been a staple of nanoparticle science where sulfur compounds are exploited as passivating/stabilizing agents and for their ability to self-assemble into well-ordered monolayers. Although thiols have been dominant in this respect,[1] sulfides are also used and may be better suited for certain applications. Dialkyl sulfides bond less strongly with Au, having bond strengths near 60 kJ mol^{-1} as compared with the 130 kJ mol^{-1} value typical of chemisorbed alkanethiol−Au bonds.[2,3] Unlike alkanethiols, where both physisorbed (∼60 kJ mol^{-1}) and chemisorbed (∼120 kJ mol^{-1}) forms have been observed, dialkyl sulfides do not readily chemisorb to Au(111) and only physisorption (∼60 kJ mol^{-1}) occurs.[3] This aspect of their chemistry is useful in nanofabrication technologies where, ultimately, removal of the passivating sulfide layer is desirable. Au nanowires formed via annealing of self-assembled nanoparticles passivated with alkyl sulfides, for example, are found to be much cleaner than those formed from alkanethiol-passivated nanoparticles.[4] More complete evaporative loss of adsorbed alkyl sulfide reduces the amount of carbonaceous deposits on nanostructures fabricated from passivated nanoparticles. The nature of monolayers formed from alkyl sulfides is also distinct from that of monolayers formed from alkanethiols; the layers tend to be more disordered.[2] The packing density, tilt, and degree of order in such monolayers reflect a delicate balance between molecule−surface interactions and lateral van der Waals forces acting between adsorbed molecules. These same forces have an impact on the adsorption and desorption kinetics, the lateral diffusion of molecules across the metal surface, and the rate of self-healing of film defects.[5] Functionalizing the termina of the alkyl chains may allow control over these forces and over many film properties. Functional groups also afford an opportunity to direct the self-assembly of multilayer structures.

The interaction of functionalized dialkyl sulfides with nanoparticles is also a topic of great interest in military defense sciences. In this context, sulfur mustard (2,2′-dichloroethyl sulfide) is the sulfide of interest and the development of materials as effective barriers to mustard permeation is the objective. Typically, such protective materials are carbon-based and operate via a high adsorption capacity. An inherent flaw in this approach is the potential for re-emission (off-gassing) of adsorbed mustard and the associated risk of subsequent exposure. To circumvent this problem, self-detoxifying materials that break down toxic gases into nonharmful reaction products are being developed. Recently, metal-oxide nanoparticles have been shown to be effective at breaking down mustard into nontoxic reaction products.[6,7] Nanoparticles have many properties that make them attractive for protective materials development including their unique size-dependent and shape-dependent reactivity as well as their large surface areas and adsorption capacity.[8−10] Nanoparticles are also readily functionalized, thus providing a means to control interaction with polymer matrixes such that well-bound, well-dispersed, nanocomposite materials suitable as protective barriers can be generated.

In this paper, we examine the effectiveness of Au nanoparticles as reactive centers and/or as adsorbents. The affinity of Au for S, the nontoxicity of gold nanoparticles, and the wealth of literature available for gold nanoparticles make them highly suitable candidates for prototype protective barrier, nanocomposite materials. In such an application, irreversible adsorption and/or chemical transformation of mustard into nontoxic reaction products is desired, thus preventing permeation of mustard through the protective material. The dialkyl sulfide data cited above suggest that relatively low binding energies and high activation energy barriers preclude irreversible adsorption and dissociative adsorption, respectively. However, mustard is a halogenated compound and the presence of Cl at the chain termina may affect the adsorption energetics. In this paper, we use gas-phase experiments to determine the binding energy of chloroethyl ethyl sulfide (a simulant of sulfur mustard) and 2,2′-dichloroethyl sulfide (sulfur mustard) to gold nanoparticles and determine the effect of chlorination of dialkyl sulfides on the adsorption to gold.

Surface-plasmon resonance (SPR) spectroscopies are highly sensitive, surface-specific techniques that exploit the sensitivity of nanoparticle SPRs to changes induced via interaction of the particle with adsorbed species. In absorption (extinction) spectroscopy, shifts in the peak position associated with the SPR most commonly reflect changes in the dielectric function of the surrounding medium accompanying the adsorption of molecules to the nanoparticle surface. The technique has proven effective for the study of adsorption kinetics of small molecules onto

* To whom correspondence should be addressed. E-mail: david.pedersen@drdc-rddc.gc.ca (D.B.P.); scott.duncan@drdc-rddc.gc.ca (S.D.).

10.1021/jp0538316 CCC: $30.25 Published 2005 by the American Chemical Society
Published on Web 11/16/2005

gold[11] and for the measure of sticking coefficients and activation energy barriers for alkyl-thiol adsorption onto gold.[12] An advantage of the technique is that it works equally well in solution- and gas-phase environments. Another advantage is its sensitivity which routinely pushes 10^{-15} M.[13] Recent work reports the dark-field variant of SPR spectroscopy as having zeptomolar sensitivity.[14] Haes and Van Duyne have outlined an approach for quantification of SPR data and constructed a Langmuir isotherm for an adsorption process.[13] We use an analogous approach in this paper, constructing the Langmuir isotherms for the adsorption of chloroethyl ethyl sulfide (ClEES) and sulfur mustard on gold-nanoparticle films. The focus is on ClEES, although some sulfur mustard data have been acquired as well. From the data, binding energies of these molecules with gold nanoparticles have been extracted and the effect of chlorination of the termina of the dialkyl moiety determined.

2. Experimental Section

A 2.0 mM stock solution of hydrogen tetrachloroaurate(III) ($HAuCl_4$) was prepared. The reducing agent was a 2.0 mM solution of sodium citrate. Initially, the reduction of the gold chloride salt was carried out in a 50 mL beaker using the following components: 9.75 mL of distilled water, 0.25 mL of stock gold chloride solution, and 10 mL of reducing agent stock solution. This procedure was also scaled up by a factor of 10 without any problems. Following mixing, the beaker containing the gold chloride salt and reducing agent was placed on a stirring hot plate pre-set to heat the solution to 348 K at a gentle stir. Within 10−20 min, the color of the solution changed from clear to mauve. Further heating caused the solution to become more red in color. Heating/stirring was continued until no further color change was observed. The final maximum of the SPR absorbance peak varied between 518 and 520 nm and required 30−40 min of cumulative heating. The final solutions are stable for months or more with no measurable color change.

The quartz substrates for the gold-nanoparticle films were first functionalized with 3-aminopropyltriethoxy-silane to improve the adhesion of the gold nanoparticles to the quartz. This silanization process was found necessary to obtain a consistently high deposition and homogeneous coverage of the gold nanoparticles on the quartz. The procedure is as follows: (1) the quartz slides were soaked in acetone for 2 min and then rinsed thoroughly twice with distilled water; (2) the slides were then soaked in a 9:1 solution of distilled water and amino-silane for 5 min followed by a thorough rinsing with distilled water; (3) the final step was curing in an oven at 353 K for 30 min. Functionalized slides were stored in a sealed container with desiccant.

In a 50 mL beaker, 5.5 mL of the 2.0 mM gold stock solution was added to 4.5 mL of the gold-nanoparticle solution. A silanized quartz slide was placed vertically into the mixture and held in position with laboratory Parafilm such that it was free from touching the sides of the beaker. The quartz substrate was left to soak in the gold-salt/gold-nanoparticle solution for 8 h. This time was determined adequate to coat the substrate with a sufficient density of gold nanoparticles to obtain a strong absorbance spectrum with the UV−vis spectrometer but maintain near-monolayer coverage and minimal aggregation of the nanoparticles. Immediately upon removing the gold-nanoparticle-coated quartz substrate from the mixture, it was rinsed in a beaker containing acetone for approximately 5 s. Following this, the gold-coated slides were placed in an oven at 473 K for 60 min.

SPR response curves were measured by immersion of the film in four different organic solvents, each with a distinct refractive index. Specifically, quartz slides coated with gold nanoparticles were cut to a size that would fit into a quartz cuvette for use with the UV−vis spectrometer. The SPR response (absorbance spectrum) of the gold-nanoparticle film for each organic solvent was measured in turn, commencing either with the solvent having the highest or lowest refractive index. Following each measurement, the gold-nanoparticle film was removed from the cuvette and soaked and rinsed in a beaker containing the next solvent in the series before acquiring a new measurement in that solvent. Reference (baseline) measurements were obtained for each solvent using a blank quartz substrate.

A temperature-controlled gas cell was connected in-line with an Ocean Optics spectrometer. The stainless steel gas cell has a volume of 125 mL and is equipped with two quartz windows sealed to the cell with O-rings. The gas cell was fitted with two gas-handling lines: the first line was connected to a 131 mL glass bulb; the second line was connected to vacuum. A 50−100 mL portion of ClEES was placed in the glass bulb that was then sealed and allowed to equilibrate. A 50−100 μL portion is sufficient to ensure that a saturated vapor state is readily achieved inside the glass bulb in a short period of time. After acquiring a reference spectrum with a blank quartz substrate, a freshly baked (473 K for 60 min) gold-nanoparticle film was placed in a clip holder and positioned in the gas cell. The cell was then closed and placed under vacuum (10^{-2} Torr). Full spectra, collected every 10 s (integrated over 70−100 ms and averaged 100 times), were saved to file by the spectrometer. After ∼30 min of pumping on the cell and allowing the gas bulb to equilibrate, the cell was isolated from the vacuum and the valve separating the gas cell and the gas bulb was opened, thus transferring vapor from the bulb to the cell. The cell was then allowed to equilibrate for a few minutes. Higher vapor pressures were attained by warming the glass bulb in a water bath. At higher temperatures, the bulb was periodically vented to the atmosphere so as to prevent a pressure buildup in the gas bulb. After each experiment, the cell was placed under vacuum for at least 1 h so as to ensure no residual vapors remained in the cell. Several experiments were also completed using a known volume of 2-chloroethyl ethyl sulfide or sulfur mustard to generate a specific vapor pressure and molar concentration inside the gas cell at a specific temperature.

The sulfur mustard used in this study was synthesized in the Canadian National Single Small Scale Facility (DRDC Suffield) for the production of chemical warfare agents under the Chemical Weapons Convention. Gas chromatography−mass spectrometry determined its purity to be 96.31% 2,2′-dichloroethyl sulfide and 1.21% bis(2-chloroethyl sulfide).

3. Results

The surface-plasmon resonance for a typical gold-nanoparticle solution made according to the method described above is shown in Figure 1. As seen, a broad absorbance at visible wavelengths is observed corresponding to the optical excitation of the SPR of the nanoparticles. The wavelength corresponding to the peak of the surface-plasmon resonance, λ_{peak}, was determined to be 517.87 nm. The wavelengths associated with the maxima of the surface-plasmon peaks were determined by fitting Pearson equations (extinction $= a + b/\{1 + 4 \times [(\lambda - c)/d]^2 \times 2^{(1/e)-1}\}^e$, where a, b, c, d, and e are variables and λ is the wavelength) to the peaks and using the c parameters as the wavelengths at the maxima. Comparing the $\lambda_{peak} = 517.87$ nm value with literature values, the diameters of the nanoparticles in the stock solutions are 10 ± 5 nm.[15] Transmission electron microscope (TEM) images support these conclusions, finding an average nanopar-

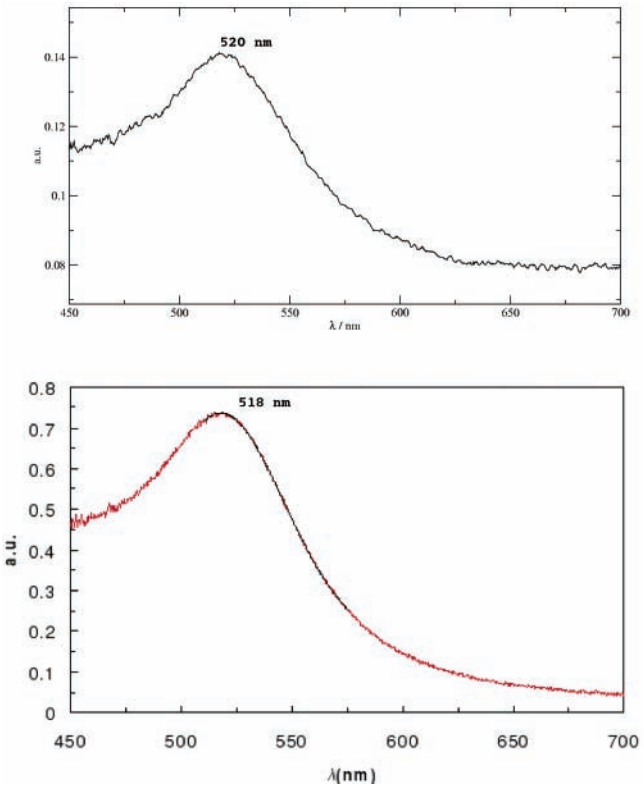

Figure 1. Surface-plasmon region of the absorption (extinction) spectrum of Au nanoparticles. The bottom is a nanoparticle solution. The red line is the experimental spectrum, and the black line is a fit of the peak of the spectrum to a Pearson equation, as described in the text. The top is a spectrum of the same nanoparticles deposited onto a quartz slide. The wavelengths corresponding to peak absorbance values are labeled. a.u. denotes absorbance units, and λ denotes wavelength.

ticle size of 14 nm (data not shown). TEM images of the nanoparticles were attained by drying a drop of solution on a TEM screen substrate.

Deposition of the gold nanoparticles onto functionalized quartz substrates manifested a shift in the SPR peak position. The spectrum of the surface-plasmon resonance for a gold-nanoparticle-coated quartz substrate made according to the method described above had a λ_{peak} value at 519.25 nm. This value is shifted from the $\lambda_{peak} = 517.87$ nm value obtained above for the nanoparticles in aqueous solution. The shift reflects the difference in the nature of the medium surrounding the nanoparticles in solution as compared to deposited on quartz. Deposition of nanoparticles onto substrates risks aggregation of the particles, which would adversely affect their sensitivity. It is self-evident that aggregates of nanoparticles would have much of the nanoparticle surface in regions of contact between particles leaving little of the nanoparticle surfaces exposed and available for adsorption of molecular species, which is a prerequisite for the resulting shift in the SPR peak position. Significant aggregation is known to cause a red shift in the SPR maximum of sufficient magnitude that the nanoparticles appear blue.[16] To the eye, our nanoparticle films made using the silanizaton/deposition procedure appear pink in color. The observed red shift in the plasmon peak position from 517.87 to 519.25 nm is relatively small considering the significant change in the nature of the medium surrounding the particles in going from an aqueous environment to their immobilization on quartz substrates. The fact that the films synthesized here are not blue indicates that no significant aggregation or multilayer deposition of the nanoparticles occurred during the deposition process onto

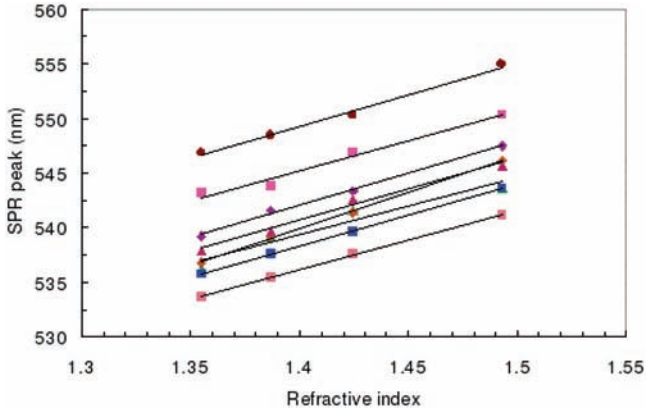

Figure 2. Response functions of gold-nanoparticle films immersed in four different liquid solvents. The different data sets correspond to different gold films. The solvents used, in order of refractive index, are acetone, *n*-heptane, dichloromethane, and toluene. The solid lines are straight-line fits of the data determined using linear regression.

the quartz substrates. The films must therefore be near-monolayer in thickness, and the nanoparticles must be well dispersed without much direct contact between them.

In Figure 2, response functions (λ_{peak} vs refractive index) of the gold-nanoparticle films are shown. Data for eight series of experiments are shown, each using a different gold-nanoparticle-coated quartz substrate. As seen, the response is linear and straight-line fits determined using linear regression are shown in Figure 2. The mean and standard error of the slope for a total of eight measurements was 57.5 ± 1.6. The spread observed in the SPR peak position for the same refractive index is likely caused by variation in the extent of adsorption of an adventitious water layer to the nanoparticles. It has been demonstrated that such water can cause a variation of ± 20 nm in the SPR peak position but that such variation in the initial SPR peak position has little or no impact on the responsiveness of the nanoparticle films.[13] Clearly, this is the case in Figure 2 where the slopes (responsiveness) are similar for different films despite the spread in SPR peak positions at a given refractive index value. The response of analogous films upon exposure to ClEES vapor is shown in Figure 3. Injection of ClEES into the gas cell resulted in an increase in the SPR peak position, λ_{peak}, that occurred in less than one spectral acquisition. Spectra were acquired every 10 s. Subsequent evacuation of the cell resulted in a decrease in λ_{peak} back to baseline values. Multiple exposure−evacuation cycles are shown in Figure 3. As seen, no irreversible change in λ_{peak} is observed and these cycles could be repeated indefinitely with no lasting effect on the nanoparticle film.

In Figure 4, the effect of varying the partial pressure of ClEES to which the nanoparticles are exposed is shown as a plot of $1/\Delta\lambda_{peak}$ (where $\Delta\lambda_{peak}$ is the difference between λ_{peak} after and before exposure to ClEES) versus the inverse of the pressure. This $1/\Delta\lambda_{peak}$ versus P^{-1} format is compatible with determining the equilibrium constant, as described below. Data collected at 298, 321, 328, and 341 K are shown. As seen, the data are compatible with the straight-line fits shown. Similar data are shown in Figures 5 and 6. In Figure 5, the Langmuir isotherm for ClEES adsorption to a gold-nanoparticle film is shown. The coverages, Θ, were determined from the position of the peak associated with the plasmon resonance in the extinction spectra of the gold-nanoparticle films. Details of this calculation are given below. The solid line is a fit of the Langmuir expression to the data (see below). Analogous data are shown for sulfur mustard in Figure 6.

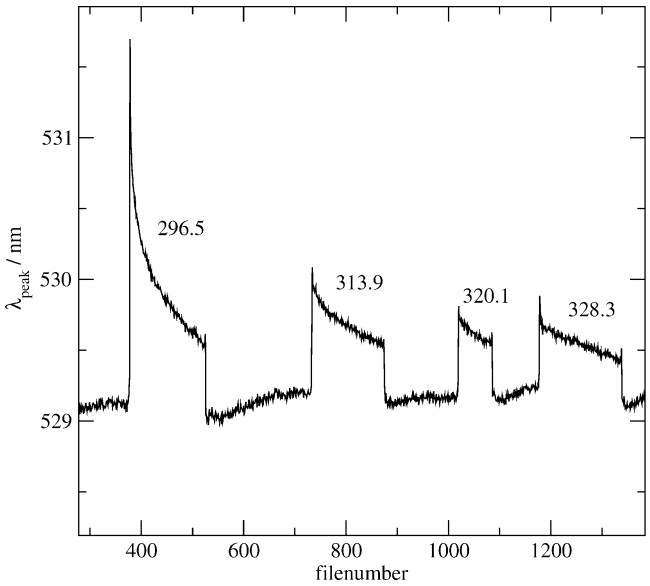

Figure 3. λ_{peak} of a gold-nanoparticle film in a gas cell shown as a function of time (given as file number where files were acquired every 10 s). The sharp increases in λ_{peak} correspond to exposure events where a pulse of ClEES vapor was injected into the cell. The sharp decreases correspond to evacuation events where the cell was placed under vacuum. The temperature of the cell is labeled on each step. The bulb temperature was kept at 343 K.

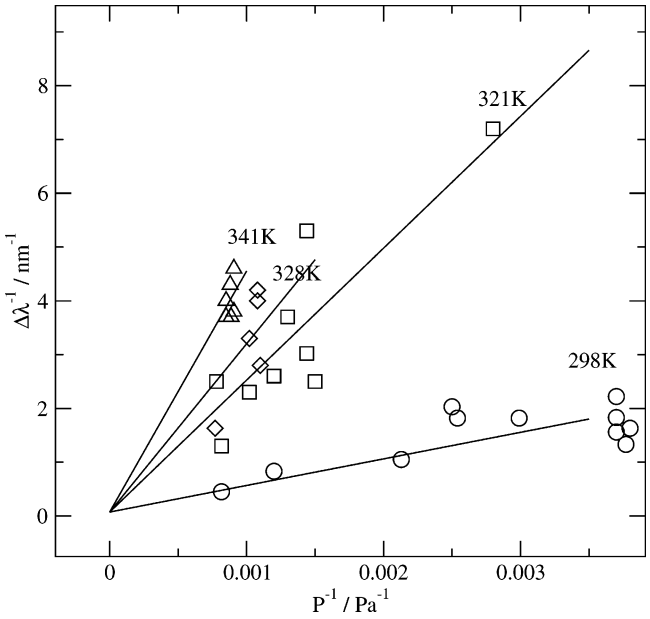

Figure 4. Plots of the inverse of the $\Delta\lambda_{peak}$ versus the inverse of partial pressure of ClEES to which gold-nanoparticle films were exposed. The temperatures at which the individual data sets were collected are labeled. The solid lines are straight-line fits of the data, determined using linear regression with the restriction that the data sets share a common *y*-intercept (see text for details).

4. Discussion

The adsorption of ClEES to gold surfaces is subject to effects associated with the presence of chlorine adjacent to the binding sulfur atom and is therefore expected to be distinct from the chemistry observed for nonhalogenated sulfides. The presence of Cl polarizes (alters the partial charge distribution of) the ClEES molecule, as is evident in the ab initio calculated Mullikan charges (see Figure 8 below). The predicted charge on the S, for example, is close to 50% less than that in the absence of Cl. As a result, both van der Waals and chemical

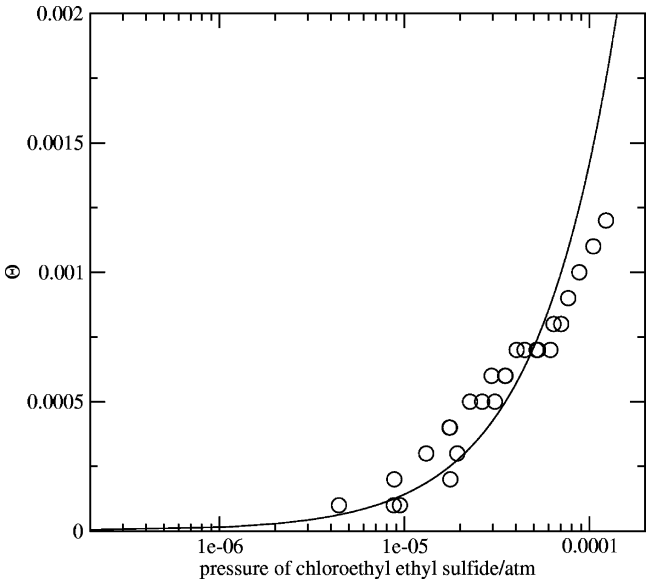

Figure 5. Langmuir isotherm for chloroethyl ethyl sulfide on a Au-nanoparticle film at 300 K. The open circles are surface coverage values, Θ, derived from measurement of the shift in the surface-plasmon resonance induced by exposure to a fixed partial pressure of chloroethyl ethyl sulfide. The solid line is a fit of the data using the Langmuir isotherm expression. See text for details.

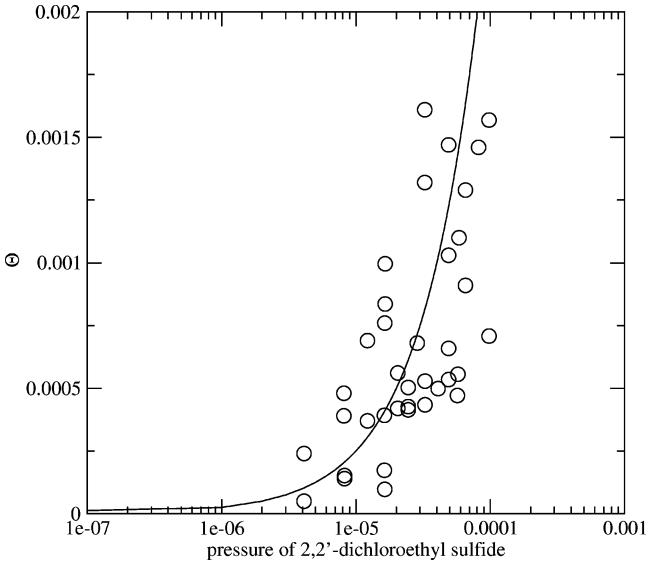

Figure 6. Langmuir isotherm for 2,2′-dichloroethyl sulfide on a Au-nanoparticle film at 300 K. The open circles are surface coverage values, Θ, derived from measurement of the shift in the surface-plasmon resonance induced by exposure to a fixed partial pressure of 2,2′-dichloroethyl sulfide. The solid line is a fit of the data using the Langmuir isotherm expression. See text for details.

interactions are expected to be affected. Chemical interactions are modest between gold and dialkyl sulfides, and evidence of chemisorption has yet to be observed. Presumably, the presence of a significant activation energy barrier along the reaction path impedes chemisorption. For ClEES, polarization is expected to modify the barrier height. Physisorption is more directly affected as a result of polarization which increases the magnitude of the van der Waals interactions. The magnitude of intermolecular interaction is reflected in the heat of vaporization. For ClEES, the heat of vaporization can be calculated using the Clausius−Clapeyron equation and the known vapor pressure of ClEES as a function of temperature[17] and is found to be 48 kJ mol^{-1}. Using the linear relationship between heat of vaporization and

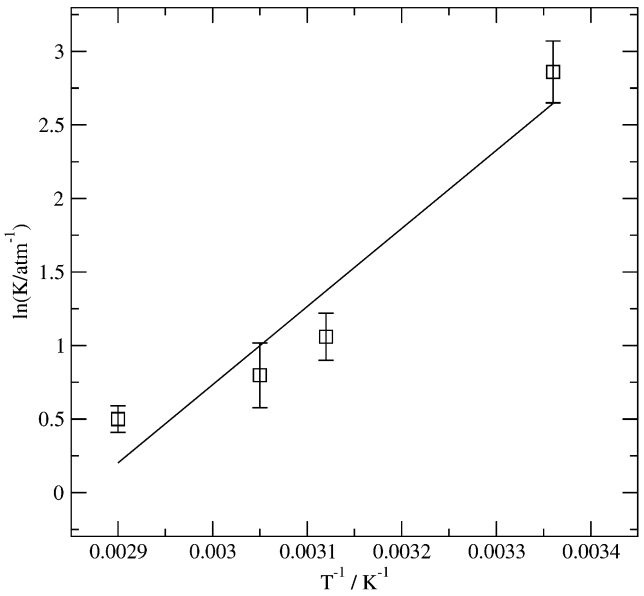

Figure 7. Van't Hoff plot for adsorption of ClEES to gold nanoparticles. *K* is the equilibrium constant for the reaction. The straight line is a linear regression fit of the data.

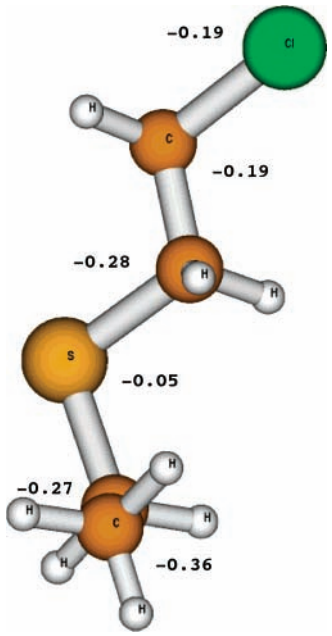

Figure 8. Geometric structure of chloroethyl ethyl sulfide as predicted by the GAMESS ab initio package. The Mullikan-analysis charges are labeled on each heavy atom.

exothermicity associated with physisorption of sulfides to gold surfaces,[3] with a 48 kJ mol^{-1} heat of vaporization, ClEES is expected to form physisorbed complexes with Au(111) with bond energies of 80 kJ mol^{-1}. That this value is significantly higher than the 68 kJ mol^{-1} bond energy of physisorbed diethyl sulfide[3] suggests an effect of the polarization due to the presence of Cl in the ClEES system.

In Figure 3, the spectroscopic response of the gold nanoparticles upon exposure to ClEES is shown. As seen, upon injection of ClEES into the gas cell containing the nanoparticles, a shift in the SPR peak position, λ_{peak}, is observed to occur in less than one spectral acquisition (~10 s). This shift reflects a change in the refractive index of the medium in the vicinity of the nanoparticles and is consistent with adsorption of ClEES to the nanoparticle surfaces. The fraction of ClEES in the injected gas is too small to effect a deviation in the refractive index of the gas from that of air, the dominant constituent, large enough to cause the observed shift in λ_{peak}. This is known from the response function of the nanoparticle films. A sampling of these is shown in Figure 2, from which it is seen that a $\Delta\lambda_{peak}$ value of the magnitude (~1 nm) observed in Figure 3 would require a change in the refractive index of the medium of 0.02. The composition-weighted average refractive index of the air−ClEES gas mixture is 1.000 02 at room temperature which is only 0.000 02 greater than the refractive index experienced by the gold nanoparticles prior to exposure to the air−ClEES mixture. This value is 3 orders of magnitude less than the 0.02 value required to manifest the observed $\Delta\lambda_{peak}$ value. Accordingly, the shifts observed in Figure 3 are not the result of changes in the refractive index of the gas-phase medium but a direct consequence of the adsorption of ClEES to the nanoparticle film. Note that injection of an air-only sample causes a negligible shift in λ_{peak}. Subsequent evacuation of the gas cell is seen to cause an instantaneous (<10 s) decrease in λ_{peak} back to baseline values corresponding to complete desorption of ClEES. Multiple exposure−evacuation cycles are shown in Figure 3, and no permanent alteration of the nanoparticles is seen. The adsorption is therefore a reversible process. The bond energy of the Au−ClEES complex must therefore be less than ~60−80 kJ mol^{-1} (calculated using a rate coefficient of 1 s^{-1}, a pre-exponential factor of 10^{10}−10^{14} s^{-1}, and the Arrhenius expression); otherwise, desorption would be so endothermic that the complete removal of ClEES from the gold surface would not occur on the 10 s time scale observed. The ~60−80 kJ mol^{-1} upper limit is comparable to the 80 kJ mol^{-1} value estimated above for physisorbed ClEES. The favorable comparison suggests that adsorption of ClEES to the nanoparticles is a physisorption process.

Aggregation of nanoparticles during the deposition process can result in porous nanoparticle films through which relatively slow diffusion of ClEES must occur before adsorption to the nanoparticle surfaces inside the pores can occur. Such diffusion processes can manifest a hysteresis effect in the reversible adsorption process. SPR spectroscopy is a very sensitive probe of the degree of aggregation, as the refractive index of the medium near the surface of nanoparticles in aggregates is significantly modified by the presence of the adjacent nanoparticles.[18] The SPR spectrum of aggregates is therefore significantly different than that of monodispersed nanoparticles. In Figure 1, a spectrum of the SPR region of a nanoparticle solution is compared with the spectrum of a nanoparticle film. The shift of λ_{peak} to the red upon deposition is expected, as the quartz substrate has a refractive index higher than that of water. The shifts observed, however, are not large enough to account for significant aggregation of nanoparticles; aggregates are known to appear blue with λ_{peak} values greater than 550 nm.[18] In light of the minimal aggregation occurring, no hysteresis is expected. The rapid decrease in λ_{peak} upon evacuation of the cell, reaching baseline values within one spectral acquisition, as seen in Figure 3, confirms that any hysteresis effects are negligible.

Following each initial exposure to ClEES, λ_{peak} is seen in Figure 3 to exponentially decay over a period of a few minutes. The extent of the decay varies and is more when the injected gas is at higher temperature and is negligible when the temperature of the injected gas is equal to the cell temperature. We can attribute this decay to cooling and the associated drop in partial pressure of ClEES in the cell. Initially, the gas arrives in the cell at the gas-bulb temperature. The gas then equilibrates

to cell temperature. With cooling, the pressure of the gas decreases. For the reversible adsorption reaction ClEES + M $\rightleftharpoons$ ClEES − M, where M represents the nanoparticle surface and ClEES − M represents the adsorbed ClEES, a decrease in the pressure of ClEES will cause desorption of ClEES from the nanoparticle surface and manifest a decrease in $\Delta\lambda_{peak}$, as observed in Figure 3. To first order, the rate of cooling will follow Newton's rate of cooling law which has an exponential form compatible with the decays observed in Figure 3. Fits of a generic exponential function (Ae^{-kt}) to the sections of data where decay is observed yield k values in the order of 0.001 s^{-1}. This is a phenomolgical rate constant reflecting both the rate of cooling as well as the rate of desorption. With decreasing temperature difference between the temperature of the injected gas and the cell temperature, the rate of cooling is observed to decrease, consistent with Newton's cooling law. Also, the rate is not affected by the cell temperature, specifically. For example, injecting 343 K gas into a 323 K cell results in a slower rate of decay than when this gas is injected into a 298 K cell. That is, the rate of decay depends on the difference between cell and gas temperature, specifically, and not on the temperature of the cell. This conclusion strongly supports the assignment of the decay observed in Figure 3 to a gas cooling process, which is an artifact of the experimental approach and not discussed further.

The equilibrium constant associated with the reversible-adsorption-of-ClEES reaction can be determined by measuring the shift in λ_{peak} observed as a function of the partial pressure of ClEES to which the nanoparticles are exposed. Formally, the shift is a linear function of the refractive index of the medium near the nanoparticles

$$\Delta\lambda_{peak} = m\Delta\eta \tag{1}$$

where $\Delta\eta$ is the change in refractive index and m is the responsiveness. The linear relationship is self-evident from Figure 2. Jung et al. have shown that for thin films the shift is proportional to the thickness of the adsorbed film[19]

$$d \propto \Delta\lambda_{peak} \tag{2}$$

For films in the monolayer regime, the refractive index is expected to change with the coverage and therefore

$$\Theta \propto \eta \propto \Delta\lambda_{peak} \tag{3}$$

For a reversible adsorption process, the coverage is related to the partial pressure of adsorbate by

$$\frac{1}{\Theta} = \frac{1}{KP_a} + 1 \tag{4}$$

where P_a is the partial pressure of the adsorbate and K is the equilibrium constant for the adsorption process. Combining eqs 3 and 4 yields

$$\frac{1}{\Delta\lambda_{peak}} = c' \times \left(1 + \frac{1}{KP_a}\right) \tag{5}$$

(where c' is a proportionality constant) from which it follows that a plot of $1/\Delta\lambda_{peak}$ versus $1/P_a$ is linear with intercept c' and slope $c'K^{-1}$. When $P^{-1} = 0$, then $1/\Delta\lambda_{peak} = c' = 1/\Delta\lambda_{max}$. $\Delta\lambda_{max}$ corresponds to immersion of the nanoparticles in liquid ClEES and, from Figure 2, has a value of 13.4 nm, from which it follows that $c' \simeq 1/13.4 = 0.073$ nm^{-1}. Using this value for c', plots of $1/\Delta\lambda_{peak}$ versus $1/P_a$ are shown in Figure 4 and are indeed linear. The slopes of these plots yielded the equilibrium constants shown in Table 1.

TABLE 1: Equilibrium Constants for the Adsorption of Chloroethyl Ethyl Sulfide to Gold Nanoparticles in the 298−340 K Temperature Range

temperature/K	K/Pa^{-1}
298	$(1.56 \pm 0.7) \times 10^{-4}$
321	$(3.06 \pm 0.3) \times 10^{-5}$
328	$(2.46 \pm 0.2) \times 10^{-5}$
340	$(1.66 \pm 0.1) \times 10^{-5}$

Equilibrium constants can also be determined by fitting the data to Langmuir isotherms. From Figure 2 (and as discussed above), it follows that the shift in λ_{max} caused by changes in the effective refractive index is given by

$$\Delta\lambda_{max} = 57.5(\eta_{eff} - \eta_{free}) \tag{6}$$

η_{eff} is the effective refractive index associated with the quartz-supported nanoparticle film on which a layer of sulfide has been adsorbed, and η_{free} is the effective refractive index of the sulfide-free film. The thickness of the adsorbed sulfide layer obviously impacts the magnitude of the shift, and the relationship between layer thickness and η_{eff} is given by[13]

$$\eta_{eff} = \eta_{free}e^{-2z/l} - \eta_{ads}\{e^{-2z/l} - 1\} \tag{7}$$

η_{free} is the effective refractive index of the film in air (i.e., $(\eta_{air} + \eta_{quartz})/2$), η_{ads} is the effective refractive index of the adsorbed sulfide, z is the thickness of the sulfide layer adsorbed to the gold-nanoparticle film, and l is the decay length associated with the exponential form assumed to describe the electromagnetic field near the particles. Substitution of eq 7 into eq 6 yields

$$\Delta\lambda - 57.5\,(\eta_{ads} - \eta_{free})(1 - e^{-2z/l}) \tag{8}$$

For ClEES, a plot of this function versus z/l increases to a maximum when z/l is ∼7; beyond ∼7, $\Delta\lambda$ remains constant. That is, SPR is only sensitive to film thicknesses where z/l is less than ≃7. We therefore associate $z_{max}/l = 7$ with $\Delta\lambda_{max}$, the maximum shift in wavelength effected by the adsorption of ClEES corresponding to a situation where the nanoparticles are completely immersed in liquid ClEES. To determine the relative depositional coverage of ClEES adsorbed to Au nanoparticles when $z \ll z_{max}$, from eq 8, it follows that

$$\frac{\Delta\lambda}{\Delta\lambda_{max}} = \frac{1 - e^{-2z/l}}{1 - e^{-2z_{max}/l}} \simeq 1 - e^{-2z/l} \tag{9}$$

Rearranging eq 9 in terms of z/l gives

$$\frac{z}{l} = -\frac{1}{2}\ln\left(1 - \frac{\Delta\lambda}{\Delta\lambda_{max}}\right) \tag{10}$$

For a Langmuir adsorption process, the surface coverage, Θ, is the ratio of the deposition in a partial layer to the deposition in a full or complete layer and is given by

$$\Theta = \frac{z}{z_{max}} = \frac{z/l}{z_{max}/l} \tag{11}$$

(compare with eq 10). Θ can be determined by solving eq 10 for z/l and dividing by z_{max}/l, which has a value of ≃7 for ClEES. $\Delta\lambda_{max}$ in eq 10 can be determined from Figure 2 and has a value of 13.4 nm for ClEES.

In Figure 5, Θ is plotted as a function of the partial pressure of ClEES to which the gold-nanoparticle film has been exposed. In accord with Langmuir, Θ is given by

$$\Theta = \frac{K \times P_a}{1 + K \times P_a} \tag{12}$$

P_a is the partial pressure of ClEES, and K is the equilibrium constant associated with the adsorption process. The solid line shown in Figure 5 is a fit of eq 12 to the data obtained by varying K exclusively. As seen, the fit is in reasonable agreement with the data. The value of K obtained for ClEES adsorption onto the gold-nanoparticle film is 14 ± 4 atm^{-1} at room temperature where the ± 4 error was determined by adjusting K to maximum and minimum values that give acceptable fits to the data. Converting the units gives $(1.4 \pm 0.4) \times 10^{-4}$ Pa^{-1} which is in agreement with the value presented in Table 1. An analogous analysis of sulfur mustard data yields the Langmuir isotherm shown in Figure 6 for which K is found to be 25 ± 5 atm^{-1}.

A van't Hoff plot constructed from the equilibrium constants given in Table 1 is shown in Figure 7. From the slope and intercept of the plot, the change in enthalpy, ΔH, and entropy, ΔS, associated with the adsorption-of-ClEES-to-gold reaction are -44 ± 9 kJ mol^{-1} and -130 ± 30 J mol^{-1} K^{-1}, respectively. The ΔH value is consistent with the 60−80 kJ mol^{-1} upper limit established above on the Au−ClEES bond energy. The 44 ± 9 kJ mol^{-1} bond energy is also lower than the 80 kJ mol^{-1} value estimated above for a physisorbed complex. The relatively low bond energy establishes that ClEES adsorbs to the gold nanoparticles via a physisorption process, exclusively. This result is consistent with previous work which has found no evidence of chemisorption of dialkyl sulfides to Au(111). By comparison, the 44 ± 9 kJ mol^{-1} value is lower than the 68 kJ mol^{-1} value found for diethyl sulfide on Au(111).[3] The difference suggests that the presence of Cl in the ClEES molecule and the associated polarization of the molecule that results has the effect of decreasing the van der Waals forces involved in bonding the physisorbed Au−ClEES complex. However, there is evidence to suggest that the bond energy of thiols physisorbed to Au surfaces is structure-dependent. Butanethiol physisorbed to Au(111) has a bond energy of 68 kJ mol^{-1} which is significantly higher than the 39.6 kJ mol^{-1} value observed on Au(110).[20] Accordingly, the difference between the 44 ± 9 kJ mol^{-1} value for ClEES on gold nanoparticles and the 68 kJ mol^{-1} value for diethyl sulfide on Au(111) may be due to differences in structure of the gold surfaces and not an effect of halogenation.

The loss of entropy associated with adsorption of ClEES to the nanoparticles is 130 ± 30 J mol^{-1} K^{-1} which is relatively high. To place the value in perspective, the structure of ClEES was determined using the GAMESS ab initio package at the Hartree−Fock level with a MINI (Huzingas 3 Gaussian minimal) basis set.[21,22] In Figure 8, the structure is shown.

Using the moments of inertia calculated by GAMESS for rotation of the molecules about the three principal axes, the change in entropy associated with loss of these motions can be calculated. Similarly, a value can be assigned to the entropy associated with loss of the three translational degrees of freedom of each molecule. These values are -76 and -171 J mol^{-1} K^{-1}, respectively. By comparison, the experimental value 130 ± 30 J mol^{-1} K^{-1} can be seen to be nearly equivalent to the predicted entropy loss corresponding to complete loss of translational motion upon adsorption. Thus, although the binding energy of ClEES to the Au nanoparticles is modest, consistent with formation of a physisorbed complex, the motion of adsorbed sulfide is severely restricted.

Assuming the entropy loss incurred upon adsorption of dichloroethyl sulfide (mustard) is comparable to that associated with adsorption of ClEES, the binding energy of sulfur mustard to gold nanoparticles can be determined. The relationship between binding energy, ΔH, and the equilibrium constant, K, is given by the Gibb's relation

$$\Delta G = -RT \ln K = \Delta H - T\Delta S \tag{13}$$

where ΔG is the change in free energy upon adsorption, R is the gas constant, and T is the temperature. Using the 25 ± 5 atm^{-1} value for K determined above and approximating ΔS as 130 ± 30 J mol^{-1} K^{-1}, eq 13 gives $\Delta H \simeq -47$ kJ mol^{-1}. This value is comparable to the -44 ± 9 kJ mol^{-1} value found for ClEES, indicating that the sulfur mustard adsorption reaction is also a physisorption process.

5. Summary and Conclusions

The ~47 and 44 ± 9 kJ mol^{-1} bond energies determined for sulfur mustard and ClEES, respectively, suggest that halogenation has little effect on the chemistry between dialkyl sulfides and gold. Bond energies of this magnitude are comparable to the 68 kJ mol^{-1} value observed for diethyl sulfide adsorption to Au(111)[3] and to the 39.6 kJ mol^{-1} value observed for butanethiol on Au(110).[20] In both of these cases, the adsorption is a physisorption process. The presence of halogen in the sulfur mustard and ClEES molecules manifests no change in bond energy large enough to warrant identification as a direct result of halogenation. The differences are small enough that they are more likely attributable to differences in the surface structure of the gold. Similarly, halogenation appears to have little impact on the chemisorption process. The ~45 kJ mol^{-1} bond energies measured are much smaller than the ~120 kJ mol^{-1} value measured for the chemisorption of thiols to Au surfaces.[3] Accordingly, there is no evidence of chemisorption of sulfur mustard or ClEES to the nanoparticles. Similar results were observed for dialkyl sulfides on Au(111), and Scoles and co-workers have suggested the presence of an activation energy barrier along the reaction path to explain the absence of any chemisorption.[3] In this context, the absence of the chemisorption of ClEES and sulfur mustard indicates that halogenation does not facilitate surmounting the energy barrier to chemisorption despite the significant change in the magnitude of the partial charge on S. Even for these short-chained species where the proximity of Cl and S is close and the impact of Cl on the S electron density is expected to be most significant, no effect is noticeable. The noneffect of side-chain substituents is similar to the noneffect of chain length on the enthalpy associated with the chemisorption of thiols on Au surfaces.[3] The Au−mustard bond energy is insufficient to ensure irreversible adsorption of mustard to the gold nanoparticles but high enough to suggest that slight modification, such as depositing the particles on a charge-donating support, may be sufficient to increase the bond strength to the point where desorption of mustard will be negligible at room temperature.

References and Notes

(1) Daniel, M. C.; Astruc, D. *Chem. Rev.* **2004**, *104* (1), 293−346.
(2) Troughton, E. B.; Bain, C. D.; Whitesides, G. M.; Allara, D. L.; Porter, M. D. *Langmuir* **1988**, *4* (2), 365−385.
(3) Lavrich, D. J.; Wetterer, S. M.; Bernasek, S. L.; Scoles, G. *J. Phys. Chem. B* **1998**, *102* (18), 3456−3465.

(4) Mendes, P. M.; Chen, Y.; Palmer, R. E.; Nikitin, K.; Fitzmaurice, D.; Preece, J. A. *J. Phys.: Condens. Matter* **2003**, *15*, S3047−S3063.
(5) Ulman, A. *Chem. Rev.* **1996**, *96*, 1533−1554.
(6) Lip, D. *J. Def. Sci.* **2001**, *6* (1), 48−54.
(7) Wagner, G. W.; Koper, O. B.; Lucas, E.; Decker, S.; Klabunde, K. J. *J. Phys. Chem. B* **2000**, *104* (21), 5118−5123.
(8) Judai, K.; Abbet, S.; Wörz, A. S.; Heiz, U.; Henry, C. R. *J. Am. Chem. Soc.* **2004**, *126* (9), 2732−2737.
(9) Cuenya, B. R.; Baeck, S.-H.; Jaramillo, J. F.; McFarland, E. W. *J. Am. Chem. Soc.* **2003**, *125* (42), 12928−12934.
(10) Jana, N. R.; Gearheart, L.; Obare, S. O.; Murphy, C. J. *Langmuir* **2002**, *18* (3), 922−927.
(11) Jung, L. S.; Campbell, C. T. *J. Phys. Chem. B* **2000**, *104* (47), 11168−11178.
(12) Jung, L. S.; Campbell, C. T. *Phys. Rev. Lett.* **2000**, *84*, 5164−5167.
(13) Haes, A. J.; Van Duyne, R. P. *J. Am. Chem. Soc.* **2002**, *124*, 10596−10604.
(14) McFarland, A. D.; Van Duyne, R. P. *Nano Lett.* **2003**, *3* (8), 1057−1062.
(15) Murillo, L. E.; Viera, O.; Vicuna, E.; Briano, J. G.; Castro, M.; Ishikawa, Y.; Irizarry, R.; Sola, L. In *Technical Proceedings of the 2002 International Conference on Computational Nanoscience and Nanotechnology*; ICCN: Puerto Rico, 2002; Chapter 16.
(16) Lazarides, A. A.; Schatz, G. C. *J. Phys. Chem. B* **2000**, *104* (3), 460−467.
(17) Bennet, S. R. e. a. *Environmental Hazards of Chemical Agent Simulants*; Technical Report CRDC-TR-84055-43; Aberdeen Proving Ground, MD, 1984.
(18) Kelly, K. L.; Lazarides, A. A.; Schatz, G. C. *Comput. Sci. Eng.* **2001**, *3* (4), 67−73.
(19) Jung, L. S.; Campbell, C. T.; Chinowsky, T. M.; Mar, M. N.; Yee, S. S. *Langmuir* **1998**, *14* (19), 5636−5648.
(20) Jaffey, D. M.; Madix, R. J. *J. Am. Chem. Soc.* **1994**, *116*, 3012−3019.
(21) Schmidt, M. W.; Baldridge, K. K.; Boatz, J. A.; Gordon, M. S.; Jensen, J. J.; Koseki, S.; Nguyen, K. A.; Su, S.; Windus, T. L. *J. Comput. Chem.* **1993**, *14*, 1347−1363.
(22) Andzelm, J.; Klobukowski, M.; Sakai, Y.; Tatewaki, H. *Gaussian Basis Sets for Molecular Calculations*; Elsevier: Amsterdam, 1984.